

# Flow over an inclined flat plate

Rohin K Rajeev  
No affiliation  
Prof. Anirudh Kulkarni  
Faculty at Pandit Deendayal Energy University  
Mr. Divyesh Variya  
Ecozen Solutions Pvt. Ltd. (Ecofrost Technologies Pvt. Ltd.)

## Abstract

The objective of this project is to numerically model incompressible turbulent flow over an inclined flat-plate structure of chord length 1 m and 3% thickness using OpenFOAM, and to study the aerodynamic effects. The angle of attack of the plate with respect to the flow is 30 degrees, and the corresponding Reynolds number of the flow based on the chord length is 150000. Numerical modeling is performed using the pisoFoam solver and  $k-\omega$  SST turbulence model in OpenFOAM. The primary objective is to investigate the influence of the height of the flat plate above the ground on the flow characteristics and the aerodynamic forces acting on the plate. Furthermore, the effect of varying Reynolds numbers on the vortex shedding frequency is examined. The results obtained were compared with the experimental data from Fage and Johansen (1927).

## 1 Introduction

As the world moves towards renewable sources of energy, the sun plays an increasingly important role. Solar energy is harnessed through various techniques, such as solar panels and solar concentrators. Solar panels, also known as photovoltaic (PV) panels, use semiconductors to directly convert sunlight into electrical energy. Solar concentrators and heliostats use mirrors or lenses to focus sunlight onto a point, where it heats a working fluid that drives an alternator. A common feature in certain photovoltaic panels and solar concentrator systems is the flat plate structured panel. Therefore, it is essential to study how air flows over the inclined plate when placed close to the ground to determine the aerodynamic forces that act on it. Understanding these forces allows for the optimisation of the support structure design in terms of strength, stability, and cost.

Numerous numerical and experimental studies have been conducted on the flow over flat plates. Numerical approaches typically include Reynolds-Averaged Navier-Stokes (RANS) simulations and Large Eddy Simulations (LES), both of which are used to model turbulent flow behaviour. RANS modelling of turbulence produces less accurate results than other methods, however, cheaper computational power requirements mean that it is widely used in the industry. These previously published studies show that the flow structure around a flat plate varies significantly depending on factors such as the plate's shape, aspect ratio, size, inclination angle, and the velocity of the incoming air. In certain configurations, vortex shedding can occur, which may induce vibrations in the plate and its supporting structure. To ensure structural integrity, the support system must be designed to withstand the resulting fluctuating stresses. Additionally, the panels must be capable of resisting sudden wind gusts, which can impose high dynamic loads. Large-scale solar installations typically cover extensive ground area, and the airflow over one panel can influence the behaviour of neighbouring panels through wake interactions. Therefore, accurately determining the flow behaviour and the aerodynamic forces acting on a flat plate is essential for the safe and cost-effective design of solar energy systems.

For a flat plate placed in a freestream flow away from walls or ground, vortex shedding typically occurs

from its edges and tips. This flow behaviour is influenced by the plate's shape and aspect ratio, which affect the vortices and the wake structure. When a solid surface, such as the ground or a wall, is present beneath the plate, the flow is altered due to the ground effect. As a result, the height of the plate above the ground plays a crucial role in determining the overall aerodynamic forces acting on it. This height and the aerodynamic stresses will determine the design of the support structure required. Coefficient of moment ( $C_m$ ) will be a factor for any hinge mechanism to determine the torque required to adjust panel orientation. In some studies, along with the angle of attack, the effect of yaw angle is also investigated. Angle of attack is the angle between the plate and the oncoming flow measured vertically and the yaw angle is defined as the horizontal angle between the plate and direction of flow. Figure 1 shows how angle of attack is measured. The Reynolds number is another key parameter which affects flow separation and vortex generation. Furthermore, airflow over solar panels will also aid in its convective cooling. As more households are adopting solar panels to produce daily required energy, studying the flow over solar panels on flat roofs and inclined roofs in real world conditions is essential.

Flat plates also find another application in UAV design. An inclined flat plate is one of the simplest wing designs a UAV wing can utilise. Therefore, studying inclined flat plate in low Reynolds number flow is valuable in the design of small or micro category UAVs mainly for defence and surveillance.

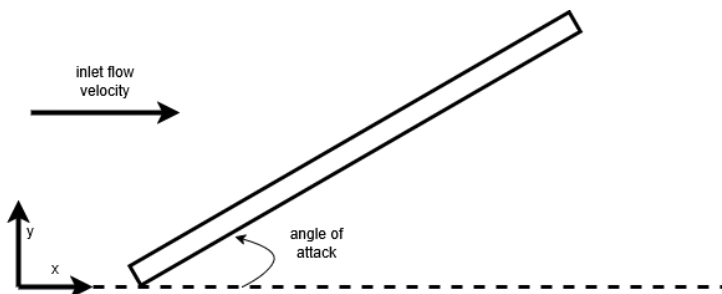


**Figure 1:** Definition of angle of attack

## 1.1 Literature review

Fage and Johannsen (1927) [1] published one of the initial studies investigating the flow of over an inclined plate. They looked at flow around a flat plate with aspect ratio of 14 where Reynolds number of the ambient flow was around 150000. The dimensions of the plate were 7 feet x 5.95 inches, with a maximum thickness of 3%. The side facing the flow was flat, and the other side tapered from the center to the tips. The pressure distribution and vortex shedding at 18 different angle of attacks were studied. They observed that the vortex shedding frequency is double at the center of the vortex street and the frequency increases proportionally to inlet velocity. The vortices are shed from the tips of the plate. As the angle of attack increased, the longitudinal spacing between the vortices increased.

Shademan and Naghib-Lahouti (2020) [2] conducted a LES study at different angles of attack and sizes of the flat plate with various Reynolds numbers to determine the effect of aspect and inclination angle. They also provide a brief summary of other published work related to flow over an inclined flat plate. Their work was validated against the results of Fage and Johannsen (1927). They observed that the angle of attack is directly proportional to the drag but inversely proportional to lift force on the plate. Furthermore, their result shows that aspect ratio and drag are directly proportional. The lift force does not change with the change in aspect ratio.

Pieris (2023) [3] reported a study on the aerodynamics of finite-span inclined flat plates in ground proximity during his PhD. In addition to angle of attack and aspect ratio of the flat plate, this study looks at the effect of the ground on the aerodynamic forces on the inclined plate. Also, yaw angle is varied to understand its effect on the flow characteristics. They observed that the ground effect is significant in cases where the plate is located 0.5 chord lengths from the ground. This study is useful for cost reduction strategies for solar panel farms.

Fadlallah [4] (2021) looks at how wind affects aerodynamic loading on a heliostat fixed at a height from the ground through a numerical analysis using the SST  $k-\omega$  and the SIMPLE algorithm. Aerodynamic forces

including lift, drag and moment about the hinge were studied.

Jafari et al., [5] observed flow over a horizontal flat plate were studied similar to the wind loading on heliostat. They found that the coefficient of lift increases with an increase in turbulence intensity. Furthermore, the lift coefficient decreases by 80% when the ratio  $H/c$  is reduced from 0.5 to 0.2 where  $H$  is the height from the ground and  $c$  is the chord length of the plate.

## 2 Problem Statement

The adoption of solar panels is increasing year after year. So, there is a need to study the aerodynamics of such a structure placed at a height from a surface. The objective of this study is to numerically model incompressible turbulent flow over an inclined flat plate structure of chord length 1m and thickness 3% placed at an angle of attack 30 degrees using OpenFOAM and to study the aerodynamic effects. The Reynolds number of the flow based on the chord length and inlet flow velocity is 150000. The project focuses on how the height from the ground affects the flow and the resulting forces on the flat plate. Furthermore, the effect of the varying Reynolds number on the vortex shedding frequency is observed.

## 3 Governing Equations and Models

The present study uses RANS equations to model the flow around an inclined flat plate. The fundamental idea behind numerical modeling using RANS is that instantaneous velocity values are divided into mean and fluctuation components [Eq.(1)], and the governing and transport equations are time-averaged or phase-averaged. The finer details of the flow are lost in the process.

In tensor notation, the instantaneous velocity  $u_i(x_j, t)$  in a turbulent flow is decomposed into a mean and a fluctuating component using Reynolds decomposition:

$$u_i(x_j, t) = \bar{u}_i(x_j) + u'_i(x_j, t) \quad (1)$$

**where:**

- $u_i$   $i = 1, 2, 3$  corresponds to the  $x$ -,  $y$ -, and  $z$ -directions respectively.
- $x_j$  represents the spatial coordinates,
- $\bar{u}_i$  is the time-averaged (mean) component.
- $u'_i$  is the fluctuating component of velocity.

Using Einstein's compact notation, the resulting Reynolds Averaged Navier Stokes (RANS) equations are expressed as follows:

Continuity equation:

$$\frac{\partial u_i}{\partial x_i} = 0 \quad (2)$$

Momentum equation:

$$\frac{\partial u_i}{\partial t} + \frac{\partial (u_i u_j)}{\partial x_j} = -\frac{1}{\rho} \frac{\partial P}{\partial x_i} + \frac{\partial}{\partial x_j} \left( \nu \frac{\partial u_i}{\partial x_j} - u_i u_j \right) \quad (3)$$

**where:**

- $\nu$ : Molecular viscosity.
- $\rho$ : Fluid density.

If the RANS equations for turbulent flow are compared to the Navier-Stokes equations for laminar flow, the only difference is the presence of the additional term  $-\overline{u_i u_j}$ , which is called the Reynolds stress tensor. Hence, this term cannot be neglected or ignored. However, these Reynolds stresses are unknown, and different turbulent models are introduced to predict them accurately.

Linear eddy viscosity models are the most commonly used turbulence models. Reynolds stresses  $-\overline{u_i u_j}$  act as an additional viscous term in [Eq.(3)]. Therefore, Reynolds stresses are represented by a quantity known as turbulent viscosity ( $\nu_t$ ) and mean velocity gradients.

Reynolds shear stresses:

$$\overline{u_i u_j} = -\nu_t \left( \frac{\partial u_i}{\partial x_j} + \frac{\partial u_j}{\partial x_i} \right) + \left( \frac{2}{3} \right) k \delta_{ij} \quad (4)$$

where  $\delta_{ij}$  is the Kronecker delta, which is defined as follows:

$$\delta_{ij} = \begin{cases} 1, & \text{if } i = j \\ 0, & \text{if } i \neq j \end{cases} \quad (5)$$

and  $k$  is the turbulent kinetic energy, given as:

$$k = \frac{\overline{u_1^2} + \overline{u_2^2} + \overline{u_3^2}}{2} \quad (6)$$

Now, the only unknown term is the turbulent viscosity ( $\nu_t$ ). Different models solve one or more transport equations for turbulent quantities such as turbulent kinetic energy ( $k$ ), turbulent kinetic energy dissipation rate ( $\varepsilon$ ), and specific turbulent kinetic energy dissipation rate ( $\omega$ ), to determine turbulent viscosity ( $\nu_t$ ). The equations for determining the  $\nu_t$  through k- $\omega$  SST model are given as follows :

$$\frac{\partial(\rho k)}{\partial t} + \nabla \cdot (\rho \mathbf{U} k) = \nabla \cdot (\rho D_k \nabla k) + P_k - \beta^* \rho \omega k \quad (7)$$

$$\frac{\partial(\rho \omega)}{\partial t} + \nabla \cdot (\rho \mathbf{U} \omega) = \nabla \cdot (\rho D_\omega \nabla \omega) + \alpha \frac{\omega}{k} P_k - \beta \rho \omega^2 + (1 - F_1) \rho \sigma_d \frac{2}{\omega} \nabla k \cdot \nabla \omega \quad (8)$$

$$\nu_t = \frac{a_1 k}{\max(a_1 \omega, SF_2)} \quad (9)$$

$$F_1 = \tanh \left( \left[ \min \left( \max \left( \frac{\sqrt{k}}{\beta^* \omega y}, \frac{500 \nu}{y^2 \omega} \right), \frac{4 \rho \sigma_\omega k}{CD_{k\omega} y^2} \right) \right]^4 \right) \quad (10)$$

$$\alpha = 0.52, \quad \beta = 0.072, \quad \beta^* = 0.09, \quad a_1 = 0.31, \\ \sigma_k = 0.85, \quad \sigma_\omega = 0.5$$

## 4 Simulation Procedure

File `/p` stores the boundary conditions related to pressure, `/U` stores the boundary conditions related to velocity. `/k`, `/omega` and `/nut` files provide constants related to the turbulence model. `BlockMeshDict` file was modified to create different meshes. `controlDict` contains the details such as solver being used and the iterations to run, `fvSchemes` contains the discretisation schemes used for simplifying differential equations that are being solved, and `fvSolution` contains details about the method used for solving the linear system of equations and residual control. OpenFOAM v2212 was utilised for this numerical analysis. The case structure for this study is as shown in figure (2).

A rectangular computational domain was chosen. The domain is divided into multiple zones to control cell size effectively and is shown in the figures (3) and (8). Cell sizes were controlled using `simpleGrading`. The domain length was taken as  $40b$ , where  $b$  is the chord length, to capture the flow wake features accurately. Therefore, the length of the domain downstream of the flat plate is longer than the upstream section. The height of the domain is  $10b$ . `BlockMesh` utility was used to create the rectangular computational mesh as shown in figure (4). For the cases with height of the plate changing, the size of the domain is changed in `blockMeshDict` file. Note : The centre of the flat plate is taken as the origin (0,0).

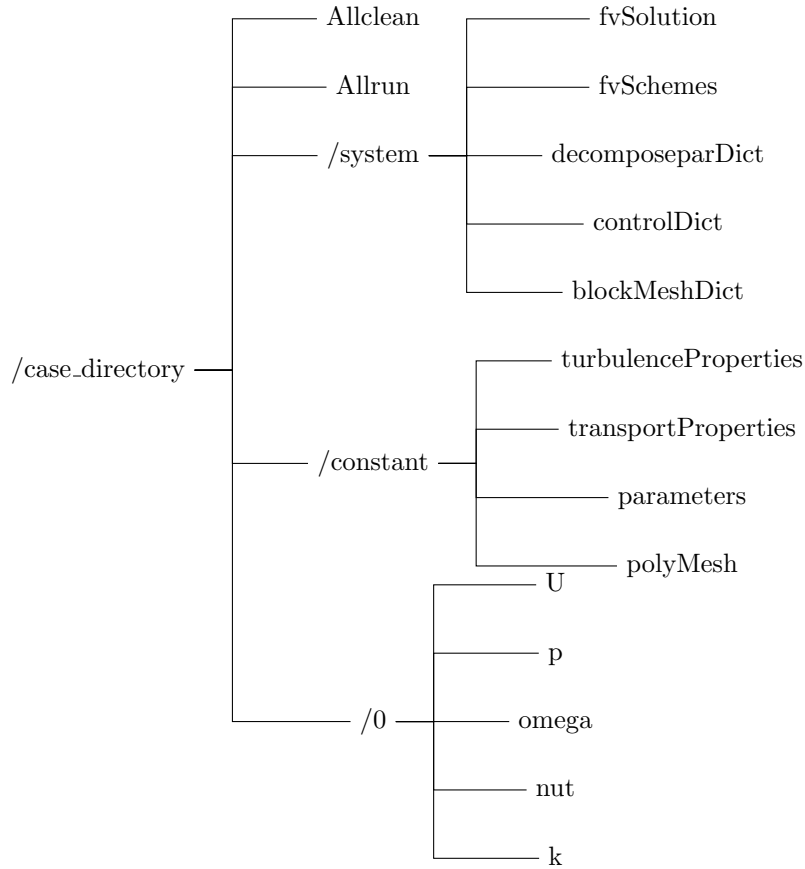


**Figure 2:** Hierarchical representation of the OpenFOAM case file structure

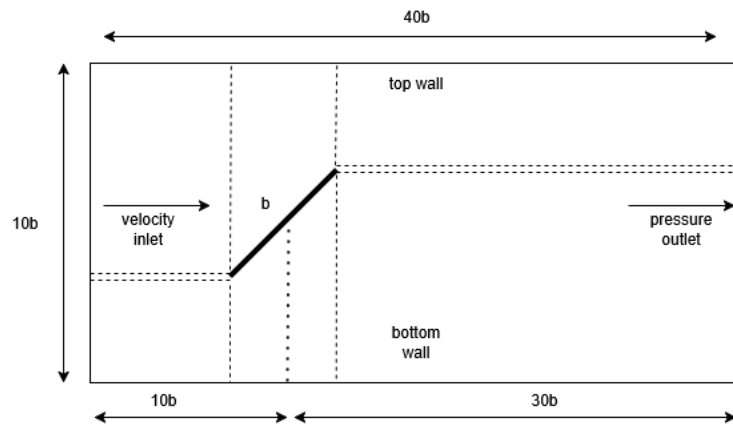


**Figure 3:** Computational domain for solver validation

The inlet velocity and outlet pressure can be set using the *parameters* file. All the cases in this study uses the  $k-\omega$  SST model. The fluid is assumed to be air at 20 degree Celsius.

The discretisation schemes employed is as follows :

- ddtSchemes - Euler

- gradSchemes - Gauss linear
- divSchemes
  - `div(phi,U)` Gauss linearUpwind grad(U)
  - `div(phi,k)` Gauss limitedLinear 1
  - `div(phi,omega)` Gauss limitedLinear 1
  - `div((nuEff*dev2(T(grad(U))))` Gauss linear

In the present study, pisoFoam solver is used for a transient analysis. The solver is run until endTime of 100 with residuals set less than 1e-6. Timestep was chosen to keep the Courant number less than one, and the writeTime was chosen to fully capture the velocity variations. An initial simulation run was performed to approximate the order of vortex shedding frequency and, correspondingly, writeTime was determined. The results are output every 0.05 seconds of simulation time. In general, writeTime is fixed such that 1/writeTime is at least twice the value of the vortex shedding frequency. Forces and force coefficients were obtained using forces and forceCoeffs functions respectively, defined in the controlDict file. The following gives the details of the solver settings:

- OpenFOAM application - pisoFoam
- P solver - GAMG with GaussSeidel smoother
- U, k, nut, omega - PBiCG with DILU preconditioner
- Residual control - 1e-06
- Pressure coupling - PISO
- Relaxation factors
  - p - 0.3
  - U, k, nut, omega - 0.5

The results were visualised in Paraview. Comparison plots are generated using simple MATLAB scripts. The velocity variations at point 5b along the streamwise downstream of center of plate are then extracted using Paraview and a FFT analysis is performed. Similarly, the coefficient of pressure over the plate surface was analysed. The coefficient of lift data was sampled using a function in the controlDict file.

To make the simulation run faster, parallel processing was employed through 'decomposePar'. The decomposeParDict file provides the number of subdivisions that we require and the method to use for decomposition. In this project, the 'scotch' method was used. Once the simulation is run and completed, the original fluid domain can be reconstructed using 'reconstructPar' command. Thus, through this technique, one can take advantage of multiple core CPUs to run an OpenFOAM case. /Allclean - removes generated result files and reset case, and /Allrun - automates simulation step by step

## 4.1 Geometry and Mesh

A flat plate for chord length 'b' and thickness of 3% is the main object of study. For the current study, the chord is 1m and the thickness is 0.03m. Initially a 2D geometry is created for validation. The blockMesh utility was used to create geometry and meshing. The mesh is divided into eight blocks with hexahedra cells. The vertices of hexahedra blocks were determined, mesh zones implemented and patched such as inlet, outlet and walls in blockMeshDict file. The 'simpleGrading' function is used to create fine cells close to the plate where boundary layers are present. A finer mesh is suitable closer to the wall and coarser cell away from the walls. This balances accuracy and computational time. However, wall functions can assist in modelling boundary layer close to walls while having coarser mesh. The mesh information is stored in the polyMesh directory. Mesh quality is checked using checkMesh command. A grid independence study was later performed to ensure solution accuracy and optimal mesh. The following is a snippet from the blockMeshDict file for 510 x 84 mesh.

```

blocks
(
  hex ( 0 1 2 3 4 5 6 7) (120 40 1) simpleGrading ( 0.1 0.01 1)
  hex ( 1 8 9 2 5 12 14 6) (30 40 1) simpleGrading ( 0.1 0.01 1)
  hex ( 8 10 11 9 12 13 15 14) (360 40 1) simpleGrading ( 10 0.01 1)

  hex ( 3 2 17 16 7 6 19 18) (120 4 1) simpleGrading ( 0.1 1 1)
  hex ( 9 11 21 20 14 15 23 22) (360 4 1) simpleGrading ( 10 1 1)

  hex (16 17 25 24 18 19 27 26) (120 40 1) simpleGrading ( 0.1 100 1)
  hex (17 20 28 25 19 22 30 27) (30 40 1) simpleGrading ( 1 100 1)
  hex (20 21 29 28 22 23 31 30) (360 40 1) simpleGrading ( 10 100 1)
)

```

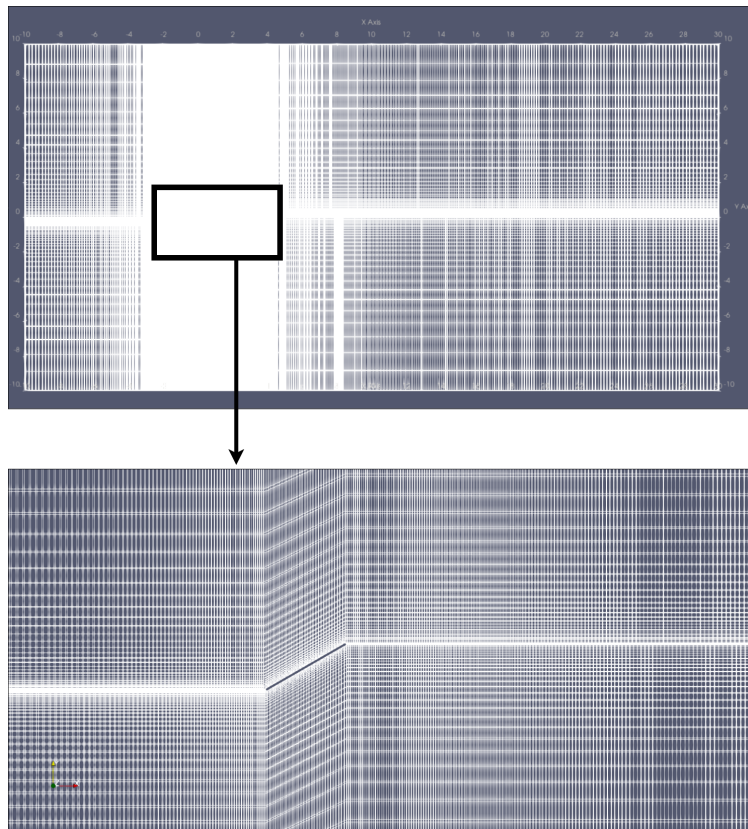


**Figure 4:** Mesh generated for solver validation with 510 x 84 cells

## 4.2 Initial and Boundary Conditions

The table 1 summarises the boundary conditions used to solve the problem. Wind velocity was provided as the inlet and the outlet as the pressure outlet. The walls were applied with no slip condition or zero velocity. The fluid properties were added to the transportProperties file and the turbulence related values were added to the turbulenceProperties file.

Boundary	Type	Velocity (m/s)	Pressure (Pa)
Inlet	Velocity Inlet	2.303	-
Outlet	Pressure Outlet	-	0
Wall	No-Slip	0	-
Plate	No-Slip	0	-

**Table 1:** Boundary conditions

The following snippet shows how the wall boundary condition for the inclined plate is defined in the blockMeshDict file. Here, "plate" is the boundary name and it is assigned a boundary type "wall". Four faces selected as given in the brackets. The numbers are the node.

```
boundary
(
  plate
  {
    type wall;
    faces
    (
      (2 6 19 17)
      (2 9 14 6)
      (9 20 22 14)
      (17 19 22 20)
    );
  }
)
```

### 4.3 Solver

OpenFOAM has different built in solvers for various cases such as steady state, transient, compressible, incompressible. This study uses the pisoFoam solver, which is a transient incompressible solver. It solves the time varying continuity equation, and momentum equation. The numerical analysis was performed at Reynolds number of 150000 using OpenFOAM. This solver is used along with the  $k-\omega$  SST turbulence model and the PISO algorithm for velocity-pressure coupling. The  $k-\omega$  model provides accuracy while not being as computationally intensive as the Reynolds stress model. Gauss linearUpwind grad(U) and Gauss linear schemes are used for discretization. It provides second order accuracy and first order accuracy respectively. First order explicit Euler method is used for temporal discretisation. However, care needs to be taken as it can produce numerical oscillations. PBiCGStab solver with DILU preconditioner is used to solving linear system. A grid independence study was performed to determine an optimal mesh containing minimal number of cells which produce accurate results in relatively shorter computational time

#### 4.3.1 Solver validation

An initial study was performed to validate the solver with Fage and Johansen [1]. A computational domain with a 30-degree inclined flat plate located in the center was created to do the study. The flow parameters and geometry were set in such a way to recreate the experiment by Fage. The inlet velocity corresponding to Reynolds number of 150000 and chord length of 1m is around 2.303m/s. The experimental data was digitised using WebPlotDigizer. [6] Five different meshes with an increasing number of cells were generated. The number of cells is multiples of 1.5. Unsteady RANS simulation was performed using the PISO solver while keeping the Courant number less than 1.

Comparison of coefficients of pressure over the plate for different meshes is performed. The results are compared with the experimental values [1] and the LES data from Shademan [2]. FFT of the velocity magnitude variation is also used for validation.

The coefficient of pressure is given by:

$$C_p = \frac{P - P_\infty}{\frac{1}{2}\rho V_\infty^2}$$

where:

- $C_p$  : Coefficient of pressure, non-dimensionalised pressure distribution over a surface
- $P$  : Local pressure at the point of interest.
- $P_\infty$  : Free-stream pressure
- $\rho$  : Density of the fluid.
- $V_\infty$  : Free-stream velocity

Here, static freestream pressure is assumed to be 0 Pa, density of the fluid is taken as 1.204 kg/m<sup>3</sup>, which is the density of air at 20 degrees and freestream velocity of the fluid as 2.303 m/s.

It is observed that the results of the RANS simulation match closely with the experimental results and LES data as seen in figure (5). The unsteady values were time averaged over 20 seconds of simulation time.

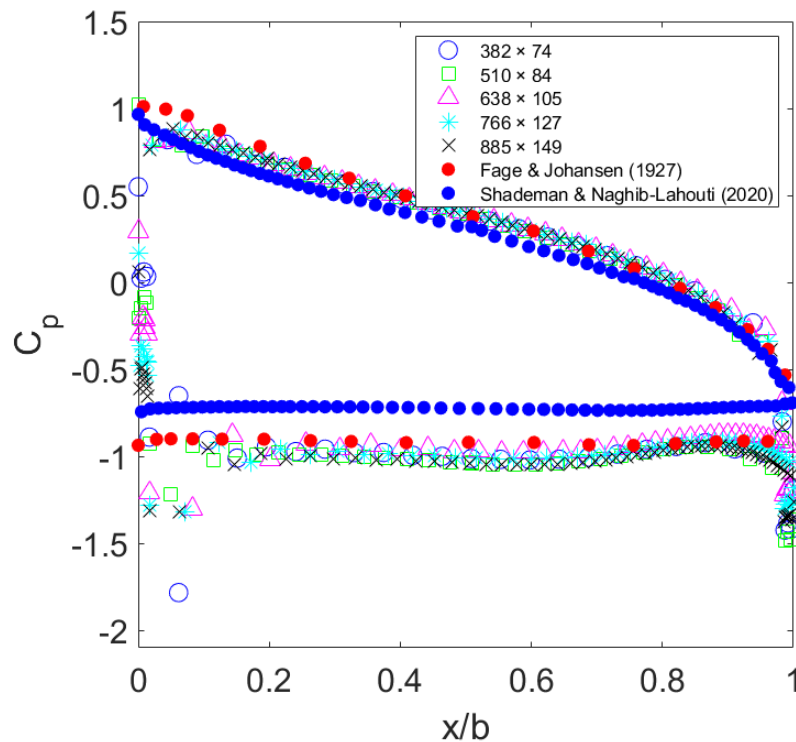


**Figure 5:** Comparison of coefficient of pressure

Strouhal number can be calculated using the following equation :

$$St = \frac{fL}{U} \quad (11)$$

where:

- $f$ : Frequency of vortex shedding (in Hz)
- $L$ : Characteristic length, here chord length of flat plate
- $U$ : Flow velocity (in m/s)

FFT in figure (6) reveals the dominant frequencies and their amplitude. As the point (5 0 0) is on the centerline behind the inclined plate, we get two dominant frequencies because vortices are shed from both tips of the plate are captured.

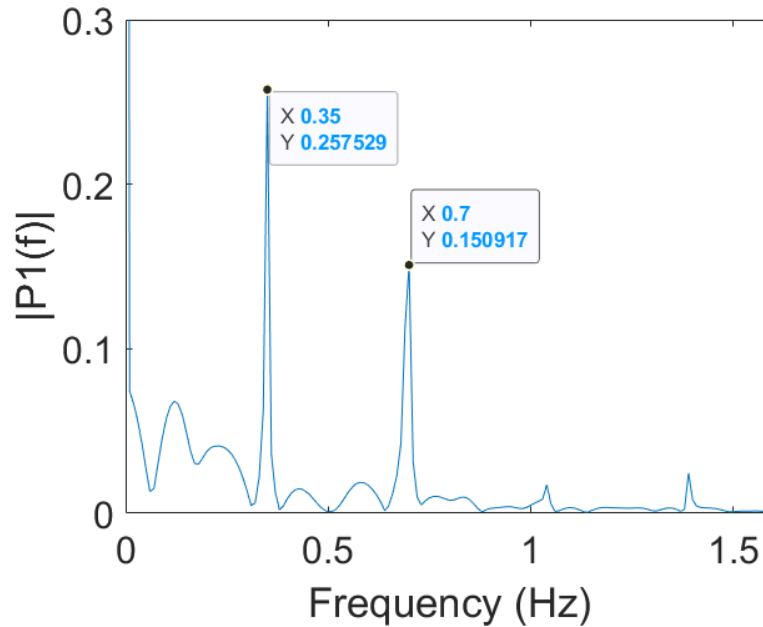


**Figure 6:** FFT of velocity magnitude at point (5 0 0) for 638 x 105 mesh

The table 2 shows the change in the vortex shedding frequency and the Strouhal number for the chosen meshes. The values velocity magnitude values were sampled at (5 0 0) which is a point in the wake of the flow and an FFT analysis is carried out. Since the values do not vary significantly with increase in number of cells, the results can be considered to be grid independent. Hence, the solver is validated, and further analysis can be performed using the same solver.

Number of cells	Vortex shedding frequency (Hz)	Strouhal number (current study)	Experimental (Fage and Johansen)	Variation percentage
382 × 74	0.68	0.295	0.307	3.90%
510 × 84	0.68	0.295	0.307	3.90%
638 × 105	0.70	0.303	0.307	1.30%
766 × 127	0.70	0.303	0.307	1.30%
885 × 149	0.70	0.303	0.307	1.30%

**Table 2:** Comparison of Strouhal number from current study and experimental data

Figure (7) shows a comparison of the velocity magnitude contour of the present study with the flow pattern of Fage[1]. We can observe strong similarities regarding how vortices emanate from the leading and trailing edges. As observed by Fage[1], there is horizontal and vertical separation between the vortices in the contour of the present study.

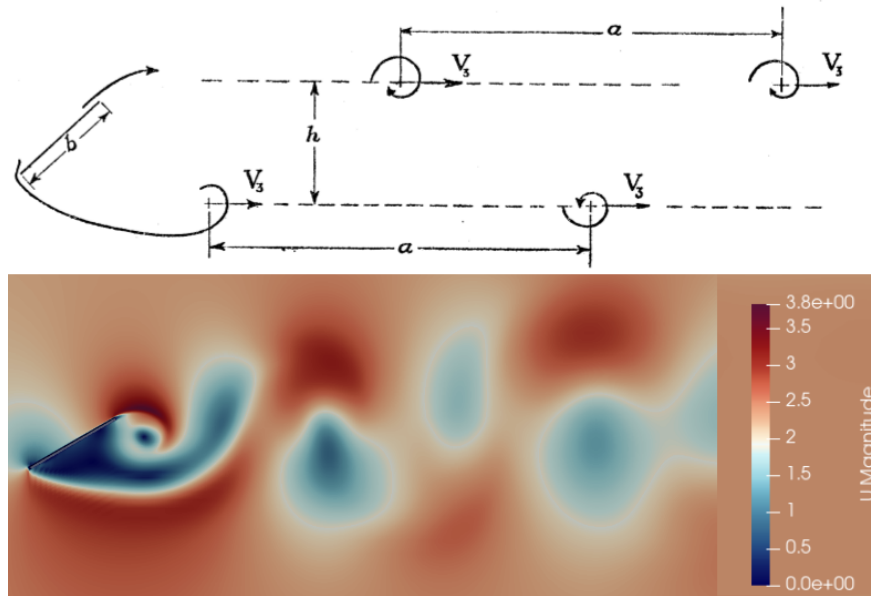


**Figure 7:** Velocity magnitude contour from present study compared to flow pattern from Fage [1]

## 5 Results and Discussions

### 5.1 Grid independence study

The figure (8) shows the new computational domain for the main study. Five different meshes, each with a different total number of cells, were generated using the blockMesh utility for the grid study. Figure (9) shows the mesh used for further analysis. The boundary conditions applied are the same as those used for the solver validation. A grid independence study was performed to determine the most suitable mesh for the analysis of the inclined flat plate fixed close to the ground.

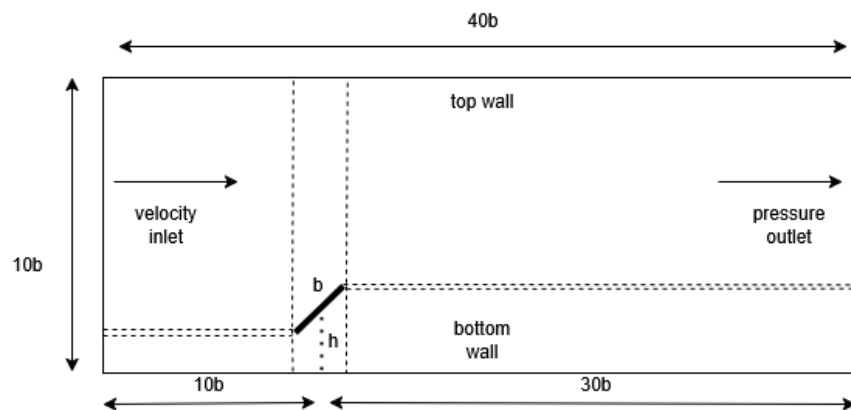


**Figure 8:** Computational domain

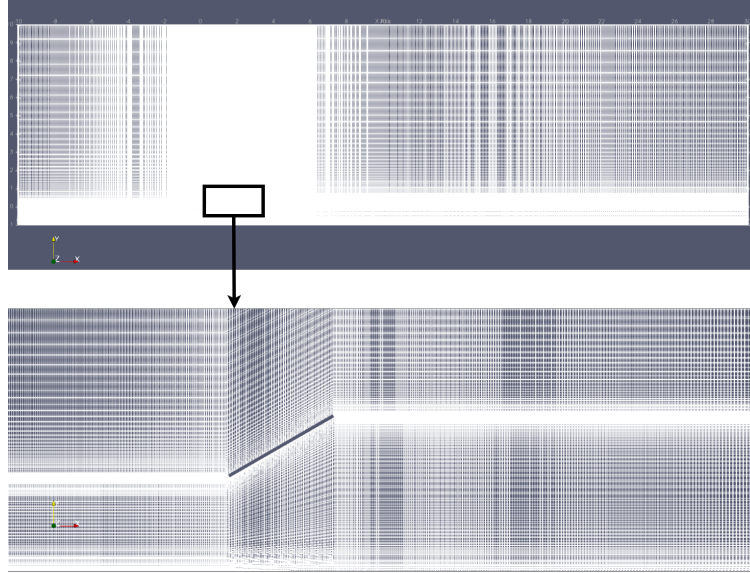


**Figure 9:** Mesh generated for  $766 \times 127$  with plate near wall

Figure (10) shows the comparison of the coefficient of pressure variation along the surface of the plate placed 1m vertically above the ground. This can be non-dimensionalised by dividing by the chord length of the plate,  $b$ . If  $h$  is the distance from the ground to the center of the plate, then  $h/b$  is the non-dimensionalised quantity. Thus,  $h/b$  is 1 for this case. The results show consistent values as the grid is refined. Furthermore, the results from this study are compared against [1] and [2] to determine how proximity to a wall affects the aerodynamic forces on the plate. It is observed that the coefficient of pressure values on the high-pressure side match well with the experimental data when the plate is positioned far from the wall. Therefore, the presence of the wall or ground close to the inclined plate does not significantly affect the high-pressure region - the surface facing the incoming flow. However, a difference is noted on the low-pressure side. The results from the current study vary by a noticeable margin. This difference in the coefficient of pressure will result in higher stress loading on the structure supporting the plate.

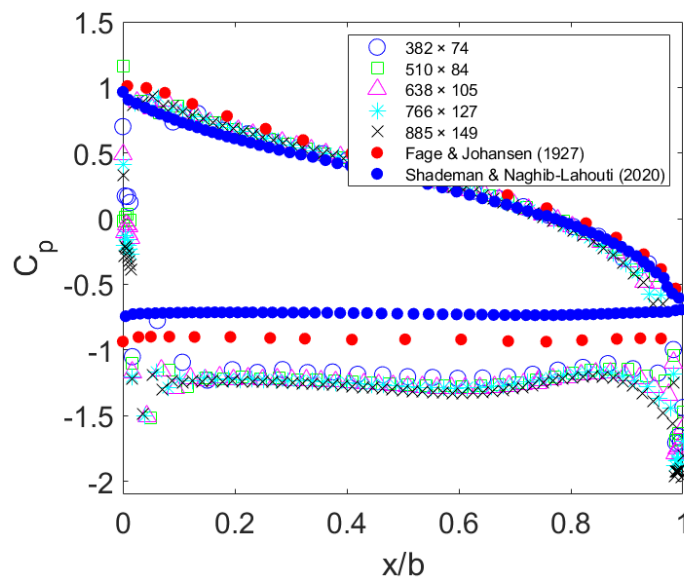


**Figure 10:** Grid independence study

Table 3 shows the variation of the Strouhal number at the point  $(5, 0, 0)$ , which lies in the wake of the plate. The Strouhal number appears to remain consistent following grid refinement, under the chosen boundary conditions, solver, and numerical settings. Therefore, for further numerical studies, the grid with  $766 \times 127$  cells is selected. It is also evident that the Strouhal numbers in this case are greater than in the case where the inclined plate was positioned farther from the wall, with  $h/b$  around 10. Compared to Fage [1], the Strouhal numbers in this study are approximately 7.5% to 10% higher. The velocity contour in figure (11) shows that the flow structures around the plate are similar to those reported in [1], where vortices are shed from both ends of the plate.

Number of cells	Vortex shedding frequency (Hz)	Strouhal number (current study)
$382 \times 74$	0.77	0.334
$510 \times 84$	0.76	0.330
$638 \times 105$	0.79	0.343
$766 \times 127$	0.78	0.338
$885 \times 149$	0.78	0.338

**Table 3:** Comparison of Strouhal number for different meshes

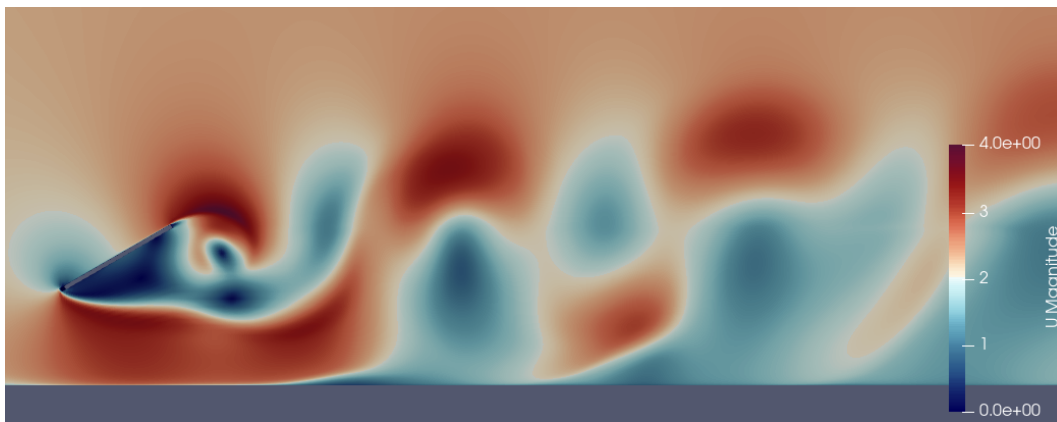
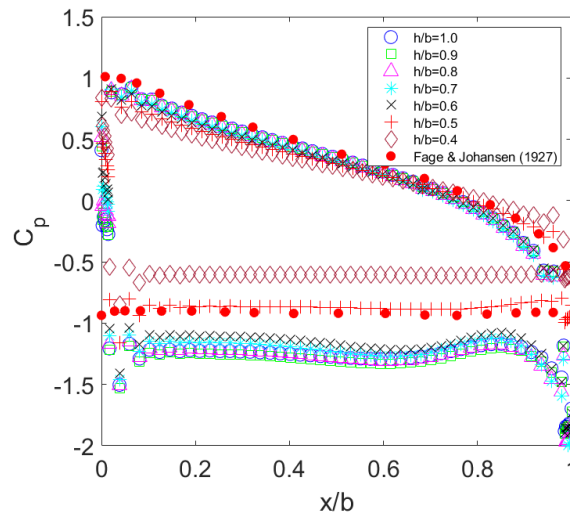


**Figure 11:** Velocity magnitude contour when plate is at  $h/b = 1$

$h/b$	Vortex shedding frequency (Hz)	Strouhal number
1.0	0.78	0.338
0.9	0.78	0.338
0.8	0.79	0.343
0.7	0.79	0.343
0.6	0.4	0.173

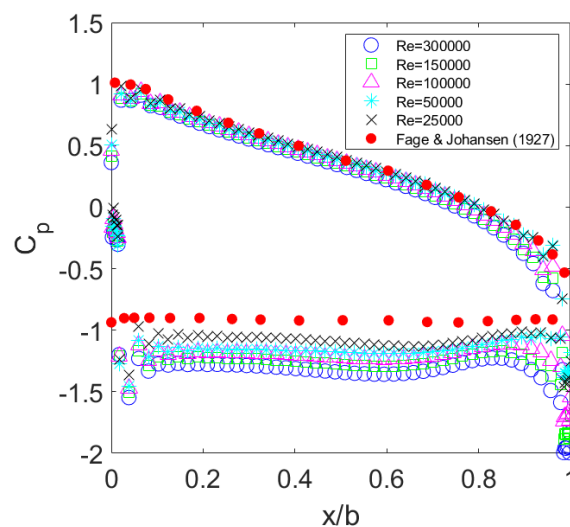
**Table 4:** Comparison of Strouhal number for different values of  $h/b$

Table (4) shows the comparison of the Strouhal numbers for different values of  $h/b$ . For  $h/b$  values between 0.7 and 1.0, the Strouhal number does not vary significantly. However, there is an approximate 50% drop in the Strouhal number when  $h/b$  decreases from 0.7 to 0.6. Note: For  $x/b = 0.4$  and  $0.5$ , the FFT does not produce a significant frequency amplitude peak, as the velocity oscillations are not strong enough.



**Figure 12:** Comparison of coefficient of pressure with varying height from wall

The figure (12) shows the coefficient of pressure over the flat plate for different cases where  $h/b$  is varied.  $h/b$  values ranging from 0.4 to 1.0 were considered. The general pattern of the  $C_p$  values matches the experimental data. However, the values on the low-pressure side vary with changes in  $h/b$ . From  $h/b = 0.7$  to 1.0, the  $C_p$  profiles are consistent with each other. As the ratio decreases from  $h/b = 0.6$  to 0.5, a significant difference is observed, and a similar deviation occurs between  $h/b = 0.5$  and 0.4. This difference in  $C_p$  profiles is likely due to the proximity of the wall. It can also be inferred that as the plate is moved closer to the wall, the suction on the low-pressure side decreases. From the perspective of a PV panel mounted on a support structure, a lower height from the ground would be advantageous, as it results in reduced aerodynamic forces acting on the panel. Consequently, the support structure can be designed to be lighter and more cost-effective.



**Figure 13:** Comparison of coefficient of pressure with varying Reynolds number at  $h/b = 1.0$

When the Reynolds number increases from 25,000 to 300,000, the vortex shedding frequency increases proportionally as seen in table 5. This is consistent with the findings of Fage [1]. Therefore, the presence of a

wall close to the plate (at  $h/b = 1.0$ ) does not have a significant effect on vortex shedding. A minor variation in the  $C_p$  profiles can be observed on the low-pressure side. As the Reynolds number increases from 25000 to 300000, the pressure on the low-pressure side decreases, indicating increased suction of the plate towards the ground at higher flow velocities. This can be visualised in figure (13). Consequently, the aerodynamic forces that act on the support structure may increase with higher wind speeds. This factor should be considered when planning large solar farms or installing solar panels in residential settings located in windy regions.

Reynolds number	Vortex shedding frequency (Hz)	Strouhal number (current study)
25000	0.06	0.158
50000	0.1	0.132
100000	0.52	0.344
150000	0.78	0.338
300000	1.46	0.316

**Table 5:** Comparison of Strouhal number for different Reynolds numbers

$h/b$	Coefficient of lift (Cl)
1.0	-0.163
0.9	-0.164
0.8	-0.160
0.7	-0.154
0.6	-0.146
0.5	-0.121

**Table 6:** Variation of Coefficient of lift (Cl) with change in  $h/b$

$h/b$	Coefficient of drag (Cd)
1.0	0.101
0.9	0.120
0.8	0.099
0.7	0.098
0.6	0.093
0.5	0.076

**Table 7:** Variation of Coefficient of drag (Cd) with change in  $h/b$

Table 6 shows the change in the coefficient of lift with varying  $h/b$  values. Here, the positive direction of lift is assumed to be in the  $(0, 1, 0)$  direction, or vertically upward. The negative values in the figure indicate that the lift force is acting in the opposite direction. So, compressive forces might act on the flat plate vertical support structures. It is observed that the coefficient of lift Cl value decreases as the  $h/b$  ratio decreases. This indicates that the downward force caused by aerodynamic lift is reduced when the plate is placed closer to the wall. The coefficient of drag Cd values in table 7 tends to lower as  $h/b$  is reduced from 1 to 0.5, although it shows an increase from  $h/b = 1$  to 0.9. This finding further supports the observation that, ideally, a solar panel should be placed closer to the ground.

In the present study, two-dimensional (2D) flow around an inclined plate is investigated. Since turbulent eddies are inherently three-dimensional (3D) features, the complete effects on the flow cannot be fully captured in a 2D simulation. This assumption introduces numerical errors, as the flow in practical scenarios

would be three-dimensional. Therefore, the results of this study should be regarded as a reference for a more comprehensive 3D flow analysis. A grid study utilising Richardson extrapolation method can give better insight to the order of spatial accuracy being achieved and grid refinement. The findings are valid within the limitations of the mesh resolution, boundary conditions, numerical discretisation, and the solver employed. Furthermore, the  $h/b$  value was restricted to the range of 0.4 to 1.0 in this study. A broader range of  $h/b$  values may reveal further insights into flow characteristics.

As a future study, the effect of flow around two or more 2D plates placed close together can be analysed. The horizontal spacing between the plates, positioned at different vertical distances from the ground, needs to be investigated, as multiple photovoltaic panels are typically installed in close proximity. Turbulence and wake effects from the upstream panels can influence the aerodynamic performance of the downstream panels. Further studies should also include fully three-dimensional cases. In addition, similar analyses can be performed on plates with varying aspect ratios, orientations, and shapes. As more households adopt solar panels to meet their daily energy needs, it is important to study the flow over panels mounted on flat and inclined roofs. In addition, the impact of wind gusts on solar panels is another critical factor that warrants investigation.

## Acknowledgments

The author is incredibly grateful to the FOSSEE team at IIT Bombay for providing access to the HPC cluster to conduct this study. The author thanks Mr. Diyvesh Variya, Dr. Anirudh Kulkarni, Mr. Pranay Pandey and Mr. John Pinto for their guidance and support throughout the period of this project. The author is also grateful to Ecozen Solutions Pvt. Ltd. (Ecofrost Technologies Pvt. Ltd.) for providing the opportunity to work on this project. Lastly, a special thanks to Ms Payel Mukherjee, Dr Chandan Bose, and other members of the FOSSEE team for their assistance.

## References

- [1] Fage, A., & Johansen, F. C. (1927). On the flow of air behind an inclined flat plate of infinite span. *Proceedings of the Royal Society of London. Series A, Containing Papers of a Mathematical and Physical Character*, 116(773), 170-197. <https://doi.org/10.1098/rspa.1927.0130>
- [2] Shademan, M., & Naghib-Lahouti, A. (2020). Effects of aspect ratio and inclination angle on aerodynamic loads of a flat plate. *Journal of Fluids and Structures*, 94, 102976. <https://doi.org/10.1186/s42774-020-00038-7>
- [3] Pieris, S. (2023). *Aerodynamics of finite-span inclined flat plates in ground proximity* (Doctoral dissertation). University of Waterloo. <https://uwspace.uwaterloo.ca/items/123f236e-9e68-493e-b9b7-c82f4054aaf6>
- [4] Fadlallah, S. O., Anderson, T. N., & Nates, R. J. (2021). Flow behaviour and aerodynamic loading on a stand-alone heliostat: Wind incidence effect. *Arabian Journal for Science and Engineering*, 46(7303–7321). <https://doi.org/10.1007/s13369-021-05405-0>
- [5] Jafari, A., Ghanadi, F., Arjomandi, M., Emes, M. J., & Cazzolato, B. S. (2019). Correlating turbulence intensity and length scale with the unsteady lift force on flat plates in an atmospheric boundary layer flow. *Journal of Wind Engineering and Industrial Aerodynamics*, 189, 218. <https://doi.org/10.1016/j.jweia.2019.03.029>
- [6] Ankit Rohatgi, WebPlotDigitizer, <https://automeris.io>